Chemical Engineering Journal 396 (2020) 125291

Contents lists available at ScienceDirect

Chemical Engineering Journal

journal homepage: www.elsevier.com/locate/cej

Evaluation of the stability of polyacrylonitrile-based carbon fiber electrode for hydrogen peroxide production and phenol mineralization during electro-peroxone process

Guangsen Xia[a,b], Huijiao Wang[b], Juhong Zhan[b], Xiaomeng Yin[a], Xiaocui Wu[a], Gang Yu[b], Yujue Wang[b,*], Mingbo Wu[a,*]

[a] State Key Laboratory of Heavy Oil Processing, College of New Energy, College of Chemical Engineering, China University of Petroleum (East China), Qingdao 266580, China

[b] School of Environment, State Key Joint Laboratory of Environmental Simulation and Pollution Control, Beijing Key Laboratory for Emerging Organic Contaminants Control, Tsinghua University, Beijing 100084, China

HIGHLIGHTS

- Polyacrylonitrile-based carbon fiber cathode maintained high stability for H_2O_2 electro-generation.
- Carbon fiber cathode maintained high phenol mineralization efficiency during multi-cycle E-peroxone process.
- Oxidation of carbon fiber by H_2O_2 and O_3 increased the ORR activity of the carbon fiber cathode.
- Oxidation of carbon fiber by H_2O_2 and O_3 decreased the selectivity of the cathode for two-electron ORR to H_2O_2.

GRAPHICAL ABSTRACT

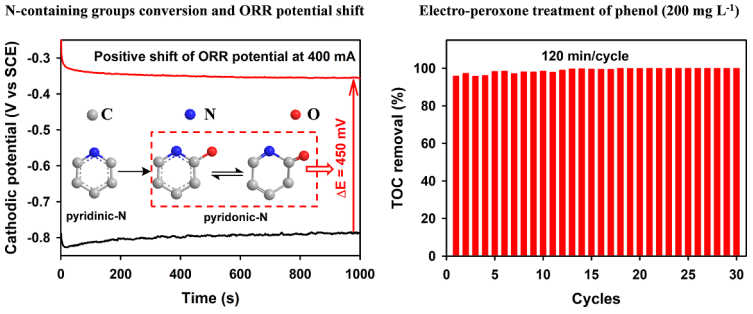

ARTICLE INFO

Keywords:
Carbon
Electro-peroxone
Hydrogen peroxide
Oxygen reduction reaction
Ozone

ABSTRACT

This study evaluated the stability of polyacrylonitrile-based carbon fiber cathode for hydrogen peroxide (H_2O_2) production and phenol mineralization during multiple cycles of electro-peroxone (E-peroxone) process. Results show that the oxidation of bulk carbon fiber by electro-generated H_2O_2 and bubbled ozone (O_3) is negligible during the E-peroxone process. Nevertheless, the carbon fiber surface was oxidized to some extent as the cathode was repeatedly used in the multi-cycle E-peroxone process. Due to the oxidation by H_2O_2 and O_3, nitrogen-containing groups on the carbon fiber surface were converted from pyridinic-N to pyridonic-N during the E-peroxone process. These changes resulted in an increase in the activity of the cathode for oxygen reduction reaction (ORR), but a decrease in the selectivity of the cathode for two-electron ORR to H_2O_2. After the carbon fiber cathode was used for 30 cycles of the E-peroxone treatment of phenol solutions, the cathodic potentials for ORR shifted positively by ~450 mV, which is beneficial to reduce the energy consumption of electrochemical H_2O_2 production. Nevertheless, the apparent current efficiency (ACE) for H_2O_2 production decreased from ~91.5% for the virgin cathode to ~48.2% for the used cathode. Despite the decrease in the ACE for H_2O_2 production, sufficient amounts of H_2O_2 could still be produced during the E-peroxone process with the used

* Corresponding authors.
E-mail addresses: wangyujue@tsinghua.edu.cn (Y. Wang), wumb@upc.edu.cn (M. Wu).

https://doi.org/10.1016/j.cej.2020.125291
Received 15 January 2020; Received in revised form 4 April 2020; Accepted 29 April 2020
Available online 01 May 2020

cathode. Therefore, complete phenol mineralization was maintained during all 30 cycles of the E-peroxone treatment of phenol solutions. These results suggest that the polyacrylonitrile-based carbon fiber is a promising cathode material for long-term E-peroxone operations.

1. Introduction

The electro-peroxone (E-peroxone) process is a novel hybrid advanced oxidation process (AOP) that is enabled by in situ electrochemically generating hydrogen peroxide (H_2O_2) from two-electron oxygen reduction reaction (ORR) during ozonation [1,2]. During the E-peroxone process, H_2O_2 is typically produced directly in the ozone contactor that is retrofitted with electrodes to produce H_2O_2 from oxygen (O_2) in the bubbled ozone and oxygen (O_3/O_2) gas mixture (i.e., ozone generator effluent) [1,3]. Alternatively, high-concentration H_2O_2 solution can be produced in electrolytes in a separate electrochemical reactor, then feed into the ozone contactor that contains the water to be treated [4]. The former approach has a simpler and more compact system, and can directly exploit O_2 in the bubbled O_3/O_2 gas as the oxygen source for ORR. On the other hand, the latter approach requires an extra oxygen source (e.g., O_2 in the off-gas of the ozone contactor) and a separate electrochemical reactor for H_2O_2 production, but allows H_2O_2 to be more stably produced with lower energy consumption in case the water that needs to be treated has low electrical conductivity or has constituents that may cause electrode fouling [4].

The electrochemical generation of H_2O_2 can have multiple beneficial effects on the water treatment performance during the E-peroxone process [2,5,6]. Due to the enhanced production of hydroxyl radical ($^{\cdot}OH$) from H_2O_2-induced O_3 decomposition, the E-peroxone process can considerably enhance the degradation and mineralization of pollutants, especially ozone-refractory pollutants, compared to conventional ozonation [7–10]. In addition, because H_2O_2 can quickly reduce hypobromous acid (a key intermediate for bromate formation in ozone-based processes) back to bromide [11], the E-peroxone process can effective reduce bromate formation during the treatment of bromide-containing water compared to conventional ozonation [12–14]. These results indicate that by exploiting O_2 that is always available at high concentrations in ozonation to electrochemically produce H_2O_2, the E-peroxone process can offer a simple and convenient way to improve the performance of existing ozonation systems for water treatment [2].

Considering the vital role of H_2O_2 in the E-peroxone process, the electrodes must be able to maintain high stability for H_2O_2 electrogeneration during water treatment [2]. Due to their low cost, excellent conductivity, high ORR activity, and other favorable characteristics, carbonaceous materials (e.g., carbon black, carbon fiber, reticulated vitreous carbon (RVC)) are the most used electrocatalysts for electrochemical H_2O_2 production in water treatment [15–20]. A variety of carbon-based electrodes have been developed and tested in the E-peroxone process for water treatment, including carbon black-polytetrafluoroethylene gas-diffusion electrode (CB-PTFE GDE), carbon felt, carbon brush, and RVC [21–27]. They generally showed good catalytic activity for H_2O_2 production during short-term evaluations. Nevertheless, the stability of the electrodes during long-term E-peroxone operations, which is critical for practical applications, has not been evaluated in previous studies [4].

During the E-peroxone process, the electrodes are exposed to high concentrations of electro-generated H_2O_2. Moreover, when the electrodes are directly installed in the ozone contactor, they can also be exposed to high-concentration O_3 bubbled in the system [23]. It is well-known that carbonaceous materials can be readily oxidized by O_3, which may lead to significant changes in their catalytic activity for ORR and other reactions (e.g., catalytic decomposition of O_3 to $^{\cdot}OH$) [15,28,29]. On the other hand, when the carbon-based electrodes are used as the cathode in the E-peroxone process, the net electrons accumulated on the cathode upon cathodic polarization may protect the carbonaceous materials from being oxidized by the oxidants (i.e., the "cathodic protection" effect) [30–32]. How these counteractive effects would influence the electrocatalytic activity of the electrodes for H_2O_2 production, as well as the entailing performance of pollutant degradation during the E-peroxone process needs to be carefully investigated.

The main objective of this study was to evaluate the stability of polyacrylonitrile-based carbon fiber electrodes during water treatment by the E-peroxone process. Polyacrylonitrile-based carbon fiber is a nitrogen-containing carbon material that can be easily manufactured on an industrial scale by high-temperature carbonization of organic fiber precursors (1200–1600 °C). Currently, polyacrylonitrile-based carbon fibers are the most important commercially available carbon fiber, accounting for about 90% of the carbon fiber market [33,34]. Its low price, high electrical conductivity, inherent nitrogen-containing structures and mass production feasibility make it a promising electrode material for ORR [35]. In this study, carbon brushes made of polyacrylonitrile-based carbon fiber were used as the cathode during multiple cycles of electrochemical generation of H_2O_2 (EGH) and the E-peroxone treatment of phenol solutions. The evolution of electrochemical properties of the electrode for H_2O_2 production, as well as the mineralization of phenol during the multiple-cycle tests were followed to evaluate the stability of the electrode for long-term operations.

2. Materials and methods

2.1. Materials and chemicals

Polyacrylonitrile-based carbon fiber (T700S, 12 K, 7 μm in diameter, 0.8 g m^{-1} in linear density) was purchased from Toray Co. Potassium titanium (IV) oxalate (CAS No. 14402-67-6), Na_2SO_4 (CAS No. 7757-82-6), NaOH (CAS No. 1310-73-2), and H_2SO_4 (CAS No. 7664-93-9) were of analytical grade (AR grade) and purchased from Beijing Chemical Works Co., China. Phenol (CAS No. 108-95-2, AR grade), potassium indigo trisulfonate (CAS No. 14402-67-7, AR grade), and H_2O_2 (CAS No. 7722-84-1, AR grade, 30 wt%) were purchased from Sigma-Aldrich. Standards of hydroquinone (CAS No. 123-31-9, HPLC grade), catechol (CAS No. 120-80-9, HPLC grade), and maleic acid (CAS No. 110-16-7, HPLC grade) were shipped from Ehrenstorfer GmbH. Oxalic acid (CAS No. 144-62-7, HPLC grade) and fumaric acid (CAS No. 110-17-8, HPLC grade) were from Fluka. Formic acid (CAS No. 64-18-6, HPLC grade) was purchased from Dukan. Methanol (CAS No. 67-56-1, HPLC grade) was from J. T. Baker. All solutions were prepared using ultrapure water with resistivity > 18 MΩ cm^{-1}.

2.2. Electrolysis experiments

2.2.1. Electrochemical system

All electrolysis experiments were conducted in an open and undivided three-electrode electrochemical reactor (9 cm × 4.5 cm × 25 cm) [23]. A carbon brush cathode made of polyacrylonitrile-based carbon fiber was used as the working electrode. The electrode potential was recorded relative to a saturated calomel electrode (SCE, Leici Co., Shanghai, China). An iridium oxide coated titanium mesh (Ti/IrO_2, 6 cm × 4 cm) anode was used as counter electrode. The carbon brush cathode and Ti/IrO_2 anode were prepared according to the procedure described previously [36,37]. The distance between anode and cathode was 1 cm. Na_2SO_4 solution (0.1 mol L^{-1}, 1 L) was used as electrolytes. All electrolysis experiments were controlled by a CHI 1140B electrochemical workstation (Shanghai Chenhua Co.). The electrochemical reactor was placed in a water bath at 20 ± 1 °C during all experiments.

2.2.2. Linear scanning voltammetry (LSV) test

LSV tests were conducted to determine the onset potentials of H_2O, H_2O_2, O_2, and O_3 reduction at the cathode. The scanning rate was 0.01 V s^{-1}. During cathodic H_2O and H_2O_2 reduction tests, a high pure nitrogen gas (99.999%) was sparged into the solution at a flow rate of 0.4 L min^{-1} to remove dissolved oxygen (DO). During O_2 and O_3 reduction tests, a pure oxygen gas (99.9%) or O_3/O_2 gas mixture (25, 45 or 90 mg L^{-1} O_3) was sparged into the solution at a flow rate of 0.4 L min^{-1}.

2.2.3. Electro-generation of H_2O_2

To evaluate the electrode stability for H_2O_2 production, the experiment of H_2O_2 electro-generation from cathodic O_2 reduction was repeated for 30 cycles using the same carbon brush electrode (each cycle was 2 h). During the experiment, a pure O_2 gas (99.9%) was continuously sparged in the three-electrode cell at a constant flow rate of 0.4 L min^{-1} using a fine aerator (average pore size of 10 μm). Meanwhile, a constant current (400 mA) was applied to drive ORR to H_2O_2. The electrolyte was 0.1 mol L^{-1} Na_2SO_4 solution, which was replaced with fresh solutions after each cycle of the experiment. The cathode that had been reused for varying cycles of electro-generation of H_2O_2 (EGH) was denoted as EGH-X (X represents the cycle number).

The evolution of H_2O_2 concentrations during the experiment was followed and used to calculate the apparent current efficiency (ACE) for H_2O_2 generation (Eq. (1)).

$$\mathrm{ACE}(\%) = \frac{nFC_{H_2O_2}V}{M_{H_2O_2}It} \times 100 \quad (1)$$

where n is the electron transfer number for one O_2 molecule reduction to H_2O_2 ($n = 2$), F is the Faraday constant (96,485 C mol^{-1}), $C_{H_2O_2}$ is the measured H_2O_2 concentration (mg L^{-1}), V is the solution volume (L), $M_{H_2O_2}$is molar mass of H_2O_2 (34.01 g mol^{-1}), I is the applied current (A), and t is electrolysis time (s).

2.2.4. E-peroxone treatment of phenol solutions

The E-peroxone treatment of 1 L phenol solution (initial concentration of 200 mg L^{-1}) was performed in 0.1 mol L^{-1} Na_2SO_4 electrolyte in the three-electrode reactor. Based on the results of previous study [23], a constant current of 400 mA was applied during the E-peroxone process. Meanwhile, an ozone-containing oxygen gas produced by passing a pure oxygen (99.9%) feed gas through an ozone generator (Tonglin Technology Co., China), then sparged in the reactor at a flow rate of 0.4 L min^{-1}. During the treatment, total organic carbon (TOC) of the solution was measured to evaluate the efficiency of phenol mineralization.

To evaluate how the extended exposure to strong oxidants (e.g., O_3 and $^{\cdot}OH$) would influence the cathode performance for pollutant removal during the E-peroxone process, the carbon brush cathode was used for 30 cycles of the E-peroxone treatment of phenol solutions (each cycle was 2 h). The cathode that had been reused for varying cycles of E-peroxone treatment was denoted as EP-X (X represents the cycle number).

2.3. Analytical methods

During the E-peroxone process, gas phase O_3 concentrations at the inlet of the reactor were monitored using an ozone detector (UV-300, Sumsun EP Hi-Tech Co., Beijing). H_2O_2 concentration was determined by a spectrophotometer at 400 nm (Dr 5000, Hitachi) using the potassium titanium (IV) oxalate method [38]. Dissolved ozone was measured using indigo method [39]. TOC was measured using TOC-VCPH analyzer (Shimadzu Co., Japan). Phenol and its transformation products (e.g., hydroquinone, catechol, oxalic acid, and formic acid) were measured using a high-performance liquid chromatograph equipped with an SPD-20A UV/Vis detector, Prominence LC-20AT pump (Shimadzu, Japan) following the protocol described previously [23].

The bulk elemental composition of carbon fibers on the carbon brush cathode was analyzed with an elemental analyzer (CE-440, Exeter Analytical, Inc., North Chelmsford, MA). The surface elemental composition and valence state of the carbon fibers were measured by X-ray photoelectron spectroscopy (XPS) analysis using an ESCALAB250Xi system equipped with Al Kα X-ray source (Thermo Fisher Scientific Inc, USA). High resolution spectra were acquired at 30 eV pass energy. XPS spectra were fitted by a nonlinear least-square curve-fitting program with the Gaussian/Lorentzian product function. The surface morphology of carbon fibers was evaluated using a field emission scanning electron microscopy (SEM) (Merlin Compact, Zeiss). X-ray diffraction (XRD) measurements were performed on an X-ray diffractometer (SmartLab system, Rigaku) with Cu Kα radiation (λ = 0.15418 nm) operating at 40 kV and 40 mA. The crystallite size of carbon fibers was calculated based on the XRD pattern and Scherrer's formula [26]. Raman spectra were taken by a spectrometer (LabRAM HR Evolution, Horiba) using a He-Ne laser at 633 nm. Fourier transform infrared spectroscopy (FT-IR) spectra was obtained using a FT-IR spectrometer (Nicolet iS10, Thermo Fisher). Brunauer–Emmett–Teller (BET) surface area was determined by N_2 adsorption method using a gas adsorption system (ASAP 2460, Micromeritics).

To estimate the electrochemically active surface area of the solid–liquid interface, the electrochemical double-layer capacitance (EDLS, C_{dl}) of the electrodes were measured using cyclic voltammetry in the potential range of 0.15–0.3 V vs. SCE at varying scanning rates [40,41]. The electrochemical impedance spectroscopy (EIS) test was conducted using a CHI 760E electrochemical workstation. The measurements were carried out in O_2-saturated 0.1 mol L^{-1} Na_2SO_4 solution with a polarization potential of 0.3 V vs SCE. The spectra were collected in a frequency range of 0.01–10^5 Hz with an amplitude of 5 mV [42].

3. Results and discussion

3.1. Cathodic reactions during the E-peroxone process

During the E-peroxone process, several reactions may occur in competition with ORR at the cathode, including water (H_2O) reduction to hydrogen (H_2), further reduction of electro-generated H_2O_2 to H_2O, and O_3 reduction to O_2 and/or $O_3^{\cdot -}$ [23]. To evaluate the catalytic activity of the carbon brush electrode for these reactions, the onset potentials of H_2O, H_2O_2, O_2, and O_3 reduction at the electrode were determined using the LSV technique under varying gas sparging conditions (see Fig. 1). In O_2-depleted solutions (sparged with 0.4 L min^{-1} N_2), no current responses were observed until the potential shifted negatively to below ca. −1.5 V vs. SCE. This observation indicates that the carbon brush cathode has a low catalytic activity for H_2O reduction, which can only occur at very low cathodic potentials [23]. In comparison, when the O_2-depleted solutions were added with 200 mg L^{-1} H_2O_2, current responses increased gradually from ca. −0.4 V vs. SCE, then exhibited a sharp increase at ca. −1.25 V vs. SCE. This finding suggests that the carbon brush also has a low catalytic activity for H_2O_2 reduction, which can only occur significantly at potentials below ca. −1.2 V vs. SCE. In contrast to the low current responses observed in O_2-depleted solutions (sparged with N_2), significantly higher current responses were observed in solutions sparged with a pure O_2 gas and an O_3/O_2 gas mixture (Fig. 1). The current responses observed at ca. −0.1 V vs. SCE in the presence of pure O_2 is attributed to O_2 reduction, whereas the current responses observed at ca. 0.9 V vs. SCE in the presence of O_3/O_2 is attributed to O_3 reduction [23].

The results shown in Fig. 1 demonstrate that O_2 can be reduced at significantly positive potentials than H_2O_2 and H_2O at the carbon brush cathode, in agreement with the previous findings that carbonaceous materials have a high ORR activity, but low H_2O_2 decomposition and H_2 evolution activity [16,43]. This finding indicates that if the carbon

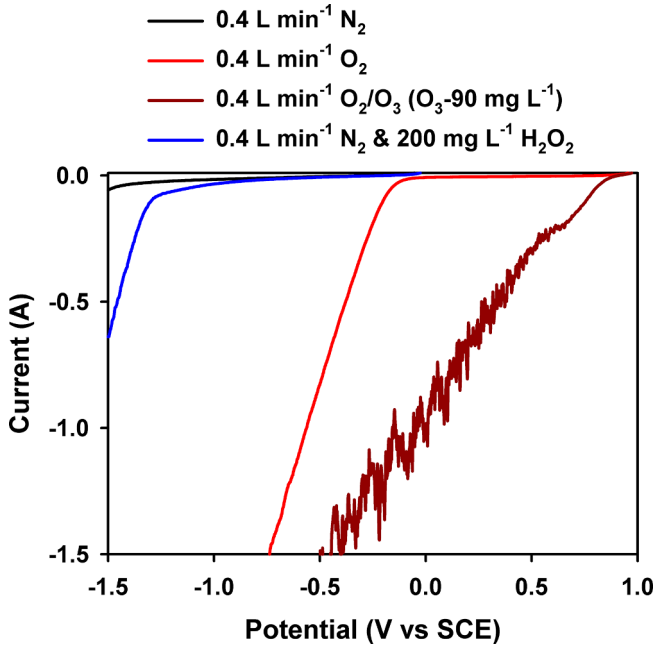

Fig. 1. LSV curves of the carbon brush cathode in Na_2SO_4 electrolyte sparged with pure N_2 and O_2 gas, and O_2/O_3 gas mixture (Na_2SO_4 concentration = 0.1 mol L^{-1}, scanning rate = 10 mV s^{-1}, gas flow rate = 0.4 L min^{-1}).

brush cathode is installed in a separate electrochemical reactor for H_2O_2 production with pure O_2 sparging, O_2 reduction will be the predominant cathodic reaction. In contrast, if the carbon brush is directly installed in the ozone reactor where an O_3/O_2 gas mixture is sparged, ORR to H_2O_2 has to compete with O_3 reduction at the cathode during the E-peroxone process. Under the conditions where cathodic O_3 reduction is limited by the mass transfer of O_3 to the cathode, ORR to H_2O_2 can occur or even dominate the cathodic reactions during the E-peroxone process [23].

Compared with other carbon-based cathodes that are commonly used for H_2O_2 production (e.g., carbon felt, CB-PTFE GDE, and RVC), the carbon brush cathode is relatively easy to prepare and scale up [44]. Moreover, the fluffy tube-brush structure of the electrode (SI Fig. S2) facilitates the close contact of carbon fibers with water, which can accelerate dissolved oxygen transfer and electron transfer between the electrode and electrolyte and thus enhance the kinetics of ORR to H_2O_2 [26,45]. Consequently, for the same mass of polyacrylonitrile-based carbon fibers (2 g), significantly higher ORR currents were achieved for the carbon brush cathode during LSV test compared to the carbon felt (see SI Fig. S3). In addition, SI Table S3 shows that under similar test conditions, a higher H_2O_2 production rate and current efficiency could be obtained with the carbon brush cathode than with the electrodes (CB-PTFE, RVC, and carbon felt) used in our previous studies (228 vs. 101–202 mg h^{-1} and 90% vs. 40–80%) [22]. These comparisons suggest that carbon brush is an effective electrode configuration for electrochemical H_2O_2 production from ORR.

3.2. Stability of the carbon brush cathode for H_2O_2 production

To evaluate the electrode stability for H_2O_2 production in the presence of pure O_2, a virgin carbon brush cathode was used for 30 cycles of electrochemical H_2O_2 production under pure O_2 gas sparging conditions. During each cycle (2 h), H_2O_2 concentrations increased continuously with increasing electrolysis time (see SI Fig. S1), which indicates that H_2O_2 is stably produced from ORR during the process. Nevertheless, the concentrations of H_2O_2 detected at the same electrolysis time declined gradually as the carbon brush cathode was repeatedly used in the multiple-cycle EGH tests (see Fig. 2 for an example of electrolysis time of 20 min). Correspondingly, the apparent current efficiency (ACE) for H_2O_2 production decreased from initially ~97% to ~79% when the carbon brush was used for 30 cycles.

The high ACE for H_2O_2 production (~97%) obtained with the virgin carbon brush cathode indicates that ORR goes essentially through the two-electron pathway to form H_2O_2 at the virgin carbon brush cathode, while the four-electron ORR to H_2O and further reduction of H_2O_2 to H_2O is negligible. However, ACEs for H_2O_2 production then decreased gradually during the multi-cycle test. This trend suggests that as the carbon brush cathode was repeatedly used for H_2O_2 electro-generation in the multi-cycle test, further reduction of H_2O_2 and/or direct four-electron ORR are gradually enhanced at the cathode, thus resulting in the decreases in ACE for H_2O_2 production.

Fig. 3a shows that as the carbon brush was reused in the multi-cycle EGH test, the onset potential of ORR shifted progressively toward more positive region. In addition, for a given potential, higher current responses were observed for the cathode that had been reused for more cycles. These observations suggest that the ORR activity of the carbon brush cathode increased gradually as the cathode was reused. Due to the increased ORR activity, the steady-state cathodic potentials of ORR at 400 mA shifted positively from ca. −0.8 V vs. SCE for the virgin cathode to ca. −0.5 V vs. SCE for the cathode used for 30 cycles of EGH test (Fig. 3c). Correspondingly, the cell voltage during electrochemical H_2O_2 production (400 mA) decreased from ~3.5 V for the virgin carbon brush cathode to ~3.2 V for the cathode used for 30 cycles (Fig. 3d). Thus, although the ACE for H_2O_2 production decreased gradually during the multi-cycle EGH test, the energy consumption for H_2O_2 production increased only slightly from initially ~5.7 to ~6.4 kWh kg^{-1} H_2O_2 as the cathode was reused for 30 cycles (see SI for the calculation). These energy consumptions correspond to ~0.38–0.42 USD kg^{-1} H_2O_2 based on the electricity cost of 0.066 USD kWh^{-1} [46], which are significantly lower than the market price of H_2O_2 stocks (~1.0–2.2 USD kg^{-1} H_2O_2 [47]. These data suggest that when the carbon brush is used to produce H_2O_2 in a separate electrochemical reactor with pure O_2 sparging, it can maintain a high stability for H_2O_2 production at competitive costs.

The above results suggest that as the carbon brush was continuously used for H_2O_2 production, its ORR activity gradually increased, while its selectivity for 2-electron ORR to H_2O_2 decreased slightly. These changes can be possibly explained by the alterations of surface properties of carbon fibers during the multi-cycle EGH test. As shown in Table 1, the bulk elemental composition of the virgin carbon brush was predominantly C (93.95 wt%) and N (4.83 wt%), with a low O content

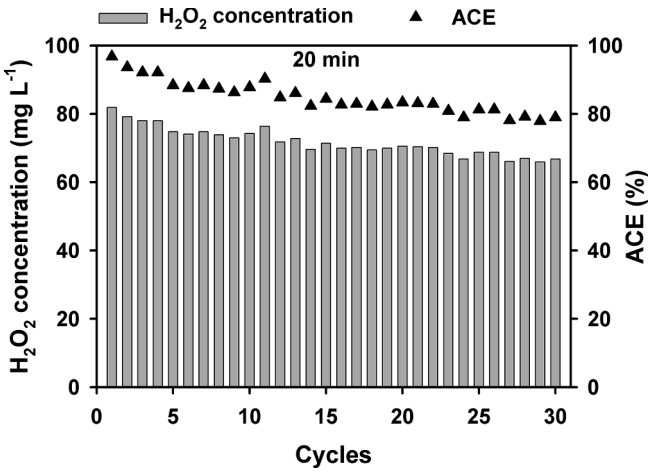

Fig. 2. Evolutions of H_2O_2 concentrations and apparent current efficiency (ACE) during the multi-cycle electrochemical H_2O_2 generation test (Na_2SO_4 concentration = 0.1 mol L^{-1}, current = 400 mA, O_2 gas flow rate = 0.4 L min^{-1}, electrolysis time = 20 min).

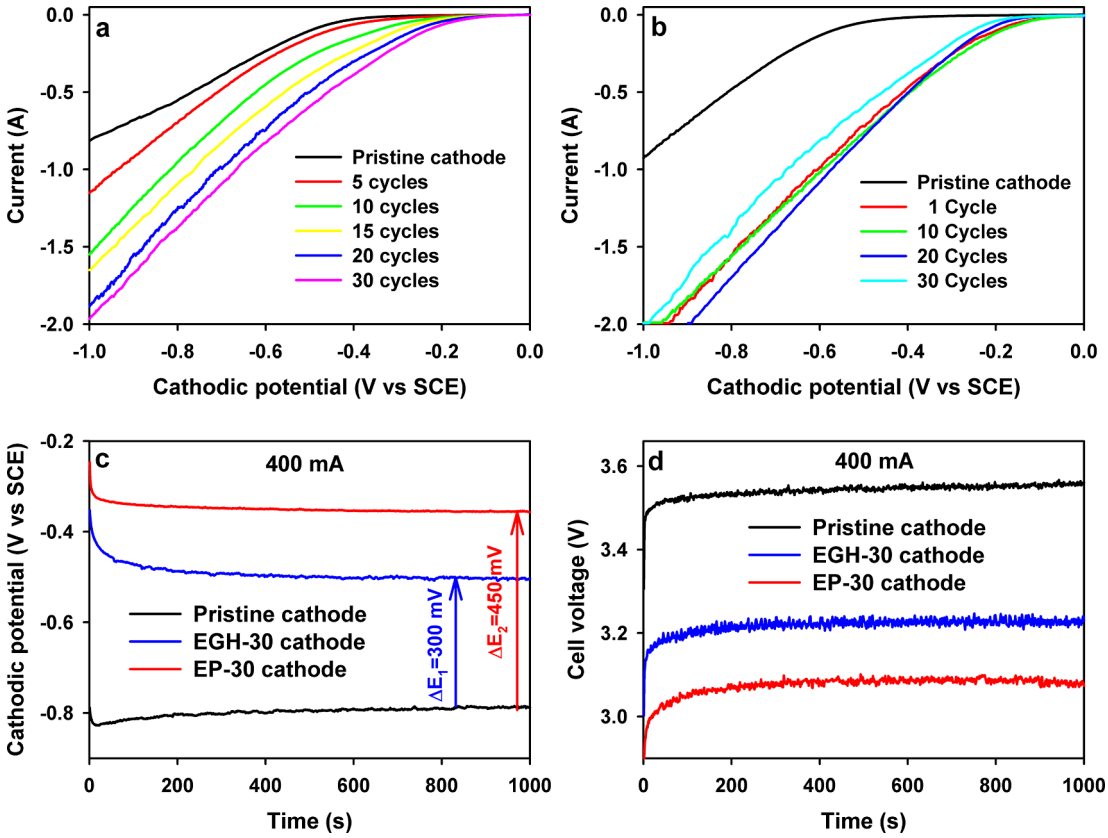

Fig. 3. (a) and (b) LSV curves of the carbon brush cathode after different cycles of electrochemical generation of H_2O_2 and E-peroxone processes (Na_2SO_4 concentration = 0.1 mol L^{-1}, scanning rate = 10 mV s^{-1}, gas flow rate = 0.4 L min^{-1}); (c) and (d) chronopotentiometry curves and cell voltage–time curves of the virgin cathode and the cathodes used for 30 cycles of electrochemical generation of H_2O_2 (EGH-30) and E-peroxone process (EP-30) cathode and EP-30 cathode (Na_2SO_4 concentration = 0.1 mol L^{-1}, current = 400 mA, O_2 gas flow rate = 0.4 L min^{-1}).

(0.52 wt%). In contrast, XPS analysis shows that the surface elemental composition had a considerably higher oxygen content (20.84 wt%), but lower C and N contents (78.33 and 0.83 wt%). The differences in the surface and bulk elemental compositions can be attributed to the fact that during commercial manufacture, carbon fibers are coated with a thin film of sizing agent (epoxy resin composed of C and O, see SI Fig. S6) [48,49]. Due to the covering of sizing agent, no N1 peaks could be detected on the surface of virgin carbon fibers during XPS analysis (Fig. 4a). In contrast, three obvious N1s peaks – pyridinic-N (N_e, 398.6 eV), graphitic-N (N_b, 400.9 eV), and pyridinic-N-Oxide (N_a, 402 eV)) - were observed on the carbon fiber surface when the sizing agent coating had been etched and cleaned by argon ion sputter before the XPS analysis (Fig. 4b).

As reported in Table 1, the bulk elemental compositions of carbon fiber remained almost constant during the multi-cycle EGH process. In addition, SEM analysis shows that there were no changes in the shape and size of the fibers after the cathode was used for 30 cycles of the EGH process (see SI Fig. S6). These observations indicate that under cathodic polarization conditions, the electro-generated H_2O_2 does not cause considerable oxidation of the bulk carbon fiber [30–32].

Table 1
Evolutions of chemical and electrochemical properties of carbon fibers on the brush cathode during the multiple cycles of electrochemical generation of H_2O_2 and E-peroxone treatment of phenol solutions.

Properties		Virgin	EGH-10	EGH-20	EGH-30	EP-1	EP-20	EP-30
Bulk elemental composition (wt%)	C	93.95 ± 0.05	94.68 ± 0.20	94.65 ± 0.36	94.26 ± 0.08	94.84 ± 0.05	94.41 ± 0.16	93.66 ± 0.33
	N	4.83 ± 0.02	4.90 ± 0.06	4.85 ± 0.17	5.00 ± 0.09	5.11 ± 0.05	4.99 ± 0.08	4.91 ± 0.18
	O	0.52 ± 0.01	0.40 ± 0.04	0.34 ± 0.03	0.51 ± 0.02	0.13 ± 0.01	0.24 ± 0.01	0.54 ± 0.09
Surface elemental composition (wt%)	C	78.33	80.92	85.21	78.69	91.41	86.83	79.94
	N	0.83	0.95	1.04	2.58	1.96	1.37	1.56
	O	20.84	18.13	13.75	18.73	6.63	11.80	18.49
Crystallite size (Å)[a]		12.7	–	–	12.3	–	–	12.2
I_D/I_G[b]		0.93	–	–	1.02	–	–	1.02
BET surface area (m^2 g^{-1})		1.1			1.6			1.8
Electrical double-layer capacitance (mF)		27	–	–	183	–	–	237
R_s (Ω)[c]		0.58	–	–	0.71	–	–	0.70
R_{ct} (Ω)[d]		28.85	–	–	0.31	–	–	0.30

[a] Measured by XRD.
[b] The ratio of peak intensity at 1360 cm^{-1} (D band) and 1580 cm^{-1} (G band) in the Raman spectra.
[c] Ohmic resistance measured by EIS.
[d] Charge transfer resistance measured by EIS.

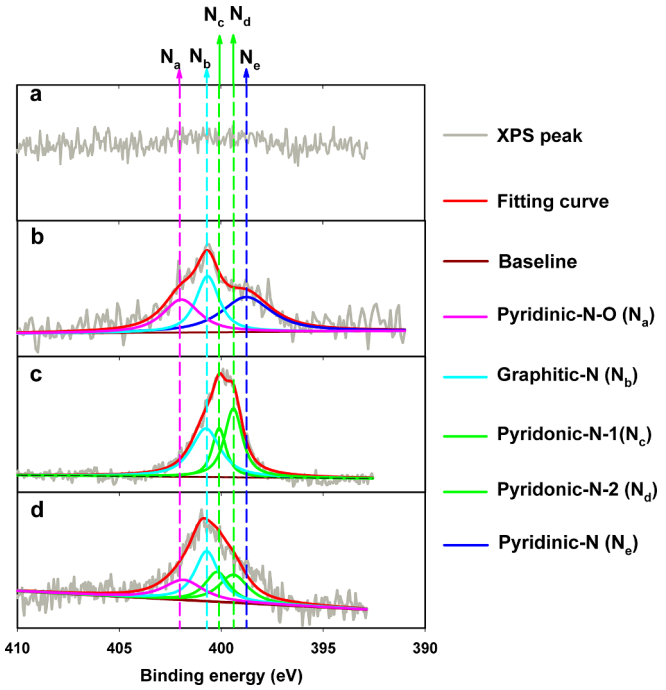

Fig. 4. N1s spectra of carbon fiber of (a) the virgin cathode, (b) the virgin cathode treated by ion sputtering, (c) the cathode used for 30 cycles of electrochemical generation of H_2O_2 (EGH-30), and (d) the cathode used for 30 cycles of the E-peroxone process (EP-30).

In contrast to the stable bulk elemental compositions, the surface elemental compositions of the carbon fibers changed evidently during the multi-cycle EGH test (Table 1). During the first 20 EGH cycles, the surface C content increased, while the surface O content decreased. The C content then decreased, while the O content increased in the last 10 EGH cycles. These changes can be probably attributed to the gradual exfoliation of epoxy resin coating from the carbon fiber surface and the subsequent oxidation of carbon fiber surface by electro-generated H_2O_2 (see SI for the SEM, FT-IR, XRD, Raman characterizations of the carbon fiber). Due to the removal of insulating epoxy resin coating and oxidation of carbon fiber surface, the electrical double-layer capacitance of the carbon fiber electrode increased considerably from 27 mF for the virgin cathode to 183 mF for the EGH-30 cathode (Table 1). These data suggest that the electrochemically active surface area of the electrode increased significantly as it was repeatedly used for H_2O_2 electro-generation (see SI Fig. S10 for more discussion) [41]. In addition, the charge transfer resistance (R_{ct}) also decreased significantly for the EGH-30 cathode compared to the virgin cathode. These changes greatly facilitate the electron transfer between the electrode and electrolyte. Consequently, the ORR activity of the carbon fiber cathode increased progressively during the 30 cycles of EGH process (Fig. 3).

Because of the exfoliation of epoxy resin coating, the N content on the carbon fiber surface increased continuously as the carbon brush cathode was reused for H_2O_2 production (Table 1). In addition, Fig. 4c shows that several N1 peaks appeared on the carbon fiber surface after the carbon brush was used for 30 cycles of H_2O_2 production. Unlike the virgin carbon fibers (Fig. 4b), the peaks of N_a and N_e disappeared after the carbon brush was reused for 30 cycles of H_2O_2 production (Fig. 4c). Meanwhile, two new peaks emerged at 399.4 eV and 400.2 eV (Fig. 4c), which are ascribed to pyridonic-N existing in the form of 2-pyridone

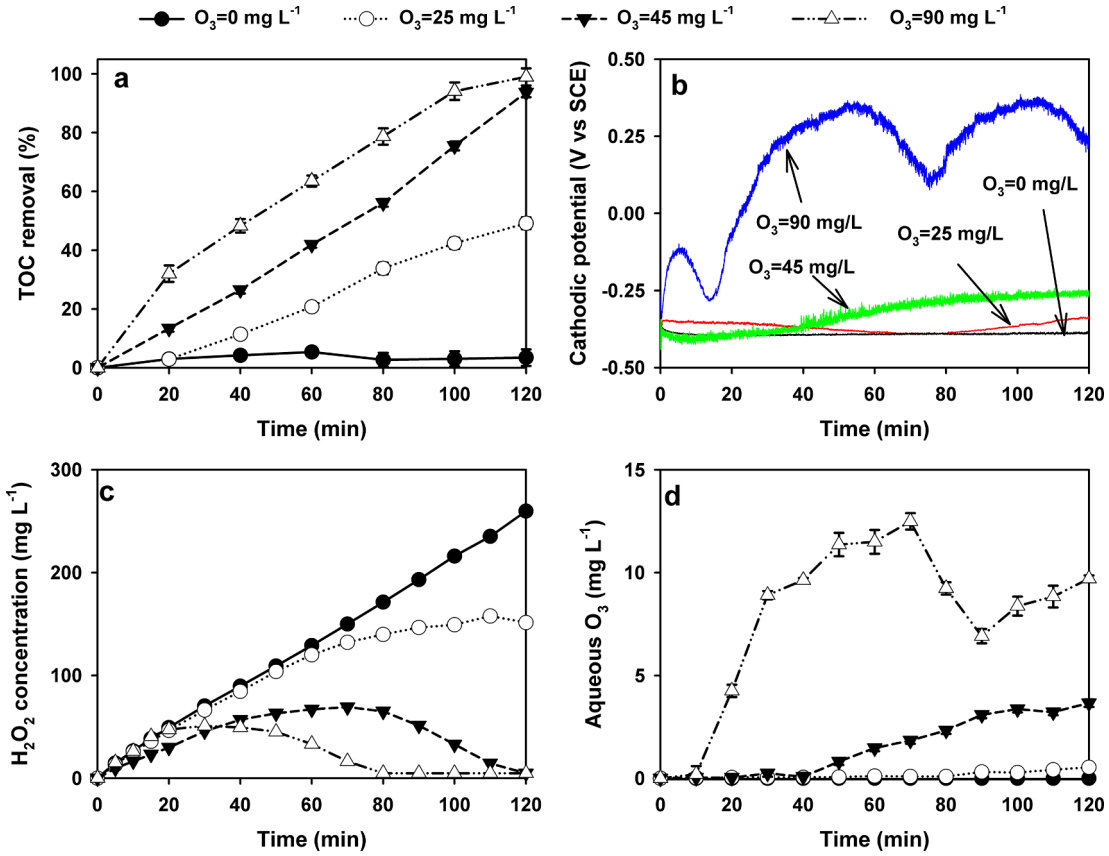

Fig. 5. Evolution of (a) TOC removal efficiency, (b) cathodic potential, (c) dissolved O_3, and (d) H_2O_2 during the E-peroxone treatment of phenol solutions (Na_2SO_4 concentration = 0.1 mol L^{-1}, current = 400 mA, gas phase O_3 concentration = 0, 25, 45 and 90 mg L^{-1}, gas flow rate = 0.4 L min^{-1}).

(N_d) and 2-hydroxyl pyridine (N_c) [35,50,51]. These changes can be probably attributed to a combined result of H_2O_2 oxidation and cathodic reduction during H_2O_2 electro-generation [35,52–54]. For example, several groups have reported that when N-doped carbon materials were used for ORR, N_a can be converted to N_e by cathodic reduction, whereas N_e could be further converted to N_c and N_d groups by H_2O_2 oxidation [35,53,54]. It is well-known that N-containing groups play a critical role in the ORR activity of carbonaceous materials [53,55,56]. For example, carbon atoms next to pyridinic-N (N_e) has been considered the ORR active sites in N-doped carbon materials and may account for the ORR activity of the virgin carbon fiber used in this study [53]. During the multi-cycle EGH test, pyridinic-N (N_e) was converted to pyrodonic-N (N_c and N_d) (see Fig. 4b and c). Compared with pyridinic-N, pyrodonic-N has a higher ORR activity, but more favors 4-electron ORR [35,50,51]. This may explain why the ORR activity of the carbon brush cathode increased progressively (Fig. 3), while the ACE for H_2O_2 production decreased gradually as the cathode was repeatedly used in H_2O_2 electro-generation (Fig. 2).

3.3. Stability of the carbon brush cathode for phenol mineralization

When carbon electrodes are directly installed in the ozone contactor for the E-peroxone process, they may be exposed to O_3 (in addition to electro-generated H_2O_2) during water treatment [23,30]. To evaluate the extent of cathode exposure to O_3 during the E-peroxone process, O_3/O_2 gas mixtures with varying O_3 concentrations were sparged during the E-peroxone treatment of phenol solutions. As shown in Fig. 5a, with increasing O_3 concentrations in the sparged O_3/O_2 gas from 0 mg L^{-1} (pure oxygen) to 90 mg L^{-1}, solution TOC was more quickly removed during the E-peroxone process. This observation can be attributed to the enhanced $^{\cdot}OH$ production from the reaction of electro-generated H_2O_2 with O_3 and/or from the cathodic reduction of O_3 at higher O_3 concentrations [23,57]. Note that the polyacrylonitrile-based carbon fiber used in this study is a non-porous material and has a small BET surface area of 1.1 m^2 g^{-1} (see Table 1). Therefore, adsorption played a negligible role in TOC removal (< 1%) during the E-peroxone treatment of phenol solutions. In addition, TOC removal by anodic oxidation (see SI Fig. S4) and H_2O_2 oxidation can also be neglected during the E-peroxone process due to the low oxygen evolution potentials of Ti/IrO_2 anodes and low reactivity of phenol with H_2O_2 [23,30,58]. Therefore, TOC was hardly removed from the phenol solution by electrolysis with pure O_2 sparging, although significant quantities of H_2O_2 were electro-generated during the process (Fig. 5c).

Although increasing O_3 concentrations in the sparged O_3/O_2 gas enhanced phenol mineralization during the E-peroxone process, this also increased the extent of cathode exposure to O_3, which can be discerned from the evolution of cathodic potentials during the processes (Fig. 5b). When pure O_2 was bubbled during electrolysis, cathodic potentials kept stably at ca. −0.38 V vs. SCE during the whole process. Meanwhile, H_2O_2 concentrations increased continuously (Fig. 5c), indicating that H_2O_2 is stably generated from ORR at the cathode. Similar phenomena were observed when an O_3/O_2 gas with 25 mg L^{-1} O_3 was sparged during electrolysis. With the lowest ozone-concentration gas sparging, aqueous O_3 concentrations were nearly undetectable during the E-peroxone process (Fig. 5d). This observation suggests that dissolved O_3 was almost completely consumed in the bulk reactions with phenol (and its ozone-reactive transformation products (TPs)) and electro-generated H_2O_2. Under such conditions, negligible amounts of dissolved O_3 can diffuse through the cathode diffuse layer to reach the cathode surface [23]. As a result, ORR to H_2O_2 remained the predominant reaction at the cathode, leading to the similar cathodic potentials as those observed when pure O_2 gas was sparged during electrolysis (Fig. 5b and d). Note that at the solution pH (~6), the second-order rate constants for the reactions of O_3 with phenol and its phenolic TPs (e.g., catechol and hydroquinone) are several orders magnitude higher than that for the reaction of O_3 with H_2O_2 [59]. Therefore, the reaction of O_3 with H_2O_2 is insignificant until phenol and its phenolic TPs have been largely transformed to ozone-resistant TPs such as oxalic acid and formic acid (see SI Fig. S2 for the evolutions of phenolic and carboxylic TPs during the E-peroxone treatment of phenol solutions). Due to the insignificant reaction of O_3 with H_2O_2 at the early phase of E-peroxone process, H_2O_2 accumulated at similar rates during the first 60 min of E-peroxone process (O_3 = 25 mg L^{-1}) and electrolysis with pure O_2 sparging (Fig. 5c). Then, H_2O_2 accumulated slower during the E-peroxone process because the consumption with O_3 became more important.

With increasing O_3 concentration in the sparged O_3/O_2 gas to 45 mg L^{-1}, phenol was more quickly mineralized during the E-peroxone process (Fig. 5a). After phenol and ozone-reactive TPs were largely converted, dissolved O_3 concentrations increased gradually from negligible levels to ~3.5 mg L^{-1} during the E-peroxone process (Fig. 5d). Corresponding to the increase of aqueous O_3 concentrations, cathodic potentials increased slowly to a plateau of ca. −0.25 V vs. SCE after 40 min of the treatment (Fig. 5b). These observations suggest that as dissolved O_3 concentrations increased, some O_3 diffused to the cathode surface, and then was reduced in competition with ORR to H_2O_2 at the cathode [23].

As O_3 concentration in the sparged O_3/O_2 gas was further increased to 90 mg L^{-1}, aqueous O_3 concentrations increased considerably after 10 min of the E-peroxone process (Fig. 5d). Coincidentally, cathodic potentials increased to > 0 V vs. SCE) after 20 min. At such positive potentials, ORR to H_2O_2 cannot proceed at the carbon brush cathode (see Fig. 1). Consistently, Fig. 5c shows that the curve of H_2O_2 concentrations undergoes an inflection at ~20 min during the E-peroxone process with the highest ozone-concentration gas sparging. These observations suggest that after ~20 min of the E-peroxone treatment of phenol solution, cathodic O_2 reduction to H_2O_2 was inhibited at the carbon brush cathode, while O_3 reduction became the dominant cathodic reactions. Notably, Fig. 5a and c show that although the electro-generated H_2O_2 was almost completely consumed after 80 min of the E-peroxone process, TOC was still quickly removed from the solution, reaching ~99% removal efficiency at 120 min. This observation suggests that cathodic O_3 reduction to $^{\cdot}OH$ plays an important role in TOC removal in the late stage of the E-peroxone process [23,25,57].

The results shown in Fig. 5 suggest that depending on reaction conditions, varied amounts of dissolved O_3 may diffuse from the bulk solution to the cathode surface during the E-peroxone process. The exposure of carbon-based cathodes to O_3 may result in electrode oxidation, and thus influence the catalytic activity of the electrode for ORR to H_2O_2 and other reactions during water treatment by the E-peroxone process. To evaluate the electrode stability under strong O_3 exposure conditions, a virgin carbon brush was used for 30 cycles of the E-peroxone treatment of phenol solution with the highest ozone-concentration O_3/O_2 gas (O_3 = 90 mg L^{-1}) sparging. Fig. 6 shows that similar TOC removal efficiencies were obtained during all cycles of the E-peroxone treatment of phenol solution. This finding suggests that the carbon brush cathode can maintain high performance for pollutant mineralization during the long-term E-peroxone operations.

Table 1 shows that the bulk elemental compositions of carbon fibers did not change considerably during the multi-cycle E-peroxone process. This observation indicates that there was no serious oxidation of the bulk carbon fiber due to the cathodic protection [30–32]. However, the surface C and N content of the carbon brush increased considerably after only one cycle of the E-peroxone treatment with the highest ozone-concentration gas sparing. Meanwhile, the surface O content decreased significantly from 20.84 to 6.63 wt%. These changes suggest that the epoxy resin coating on the carbon fibers was largely removed during the first cycle of E-peroxone treatment of phenol solution. The surface O content then increased during the following E-peroxone cycles due to the oxidation of carbon fiber surface by O_3 and H_2O_2.

XPS analysis of the N-containing groups show that after the carbon

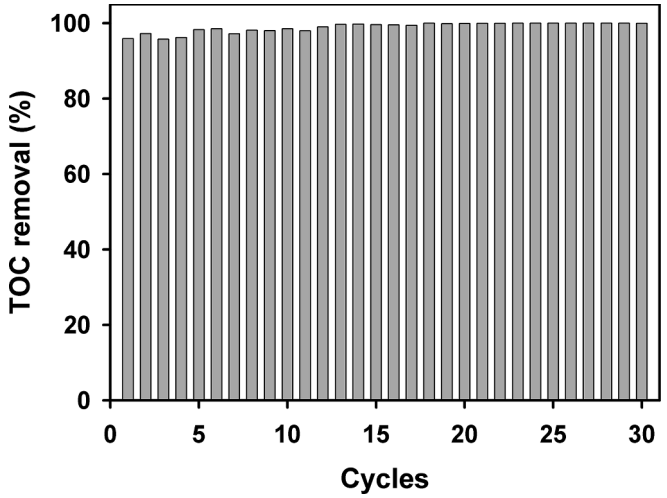

Fig. 6. Evolution of TOC removal efficiency during the multi-cycle E-peroxone treatment of phenol solutions (Na_2SO_4 concentration = 0.1 mol L^{-1}, current = 400 mA, gas phase O_3 concentration = 90 mg L^{-1}, gas flow rate = 0.4 L min^{-1}, treatment time = 2 h).

brush was used in the E-peroxone treatment of phenol solution, pyridinic-N (N_e) disappeared on the carbon fiber surface while 2-pyridone (N_d) and 2-hydroxyl pyridine (N_c) appeared (Fig. 5d), which is similar to what has been observed for the electrode used for H_2O_2 production (Fig. 5c). However, the peak of pyridinic-N-Oxide (N_a) could still be observed on the carbon fiber surface for the electrode used for the E-peroxone process (Fig. 5d). This finding suggests that the cathodic reduction of pyridinic-N-Oxide (N_a) to pyridinic-N (N_e) was partially suppressed under the strongly oxidizing conditions of the E-peroxone process due to the presence of O_3 (and other strong oxidants such as $^{\cdot}OH$).

Due to the exfoliation of epoxy resin coating and oxidation of carbon fiber surface by H_2O_2 and O_3, the EDLC of the EP-30 cathode was considerably higher than that of the virgin carbon brush cathode (Table 1). This observation indicates a substantial increase of the ECSA of the electrode. In addition, the charge transfer resistance (R_{ct}) decreased remarkably from 28.85 Ω for the virgin cathode to 0.30 Ω for the EP-30 cathode (Table 1). Corresponding to these changes, the LSV curve of ORR at the carbon brush shifted considerably to more positive region after the first cycle of E-peroxone process, then tended to be stabilizing during the following 30 cycles (Fig. 3b). In addition, the steady-state cathodic potentials during electrochemical H_2O_2 production (400 mA, pure O_2 sparging) shifted positively by ~0.45 V after the carbon brush was reused for 30 cycles of the E-peroxone process (Fig. 3c). This led to a corresponding decrease in the cell voltage during electrochemical H_2O_2 production (Fig. 3d). These observations indicate that the ORR activity of the carbon brush increased considerably during the multi-cycle E-peroxone process. Nevertheless, as shown in Fig. 7a, significantly less H_2O_2 accumulated in the solutions during electrochemical H_2O_2 production (pure O_2 sparging) with the used carbon brush cathode (EP-30) than with the virgin cathode. Consequently, the ACE for H_2O_2 production decreased considerably from ~91.5% for the virgin cathode to ~48.2% for the used cathode (Fig. 7b). These data suggests that due to the changes of surface N-containing groups, the selectivity of the carbon brush for two-electron ORR to H_2O_2 decreased substantially after it was used for the multi-cycle E-peroxone process.

Despite the decrease in the ACE of the carbon brush cathode for H_2O_2 production, high TOC removal efficiency was maintained throughout the 30-cycle E-peroxone treatment of phenol solutions (Fig. 6). This result can be probably attributed to the fact that considerable amounts of H_2O_2 could still be produced during the E-peroxone process with the used cathode (EP-30). As shown in Fig. 7a, ~40.9 mg L^{-1} H_2O_2 accumulated in the solution within the first 20 min of the 30th cycle of E-peroxone treatment. This concentration is only moderately lower than that obtained with the virgin cathode during the first cycle of E-peroxone treatment (~47.3 mg L^{-1}). Therefore, it is expected that the production of $^{\cdot}OH$ from the reaction of sparged O_3 with electro-generated H_2O_2 is generally similar during the multiple cycles of E-peroxone process. In addition, N-containing groups are often suggested as the active sites for catalyzing O_3 to $^{\cdot}OH$ during catalytic ozonation with carbonaceous materials [29,60]. During the multi-cycle E-peroxone process, N-containing groups on the carbon fiber surface are increasingly exposed due to the exfoliation of sizing agent. This may help to enhance $^{\cdot}OH$ production from O_3 reduction and thus maintain high TOC mineralization efficiency during the subsequent cycles of E-peroxone process.

The results shown above indicate that the exposure of the carbon brush cathode to O_3 during the E-peroxone process can considerably change its ORR activity and selectivity. Similar to what has been observed in electrochemical H_2O_2 production (electrolysis with pure O_2 sparging), the ORR activity of the electrode increased during the multi-cycle E-peroxone process (electrolysis with O_2/O_3 sparging), whereas the selectivity of the electrode for two-electron ORR to H_2O_2 decreased. However, the changes in the electrode properties occurred more rapidly and significantly during the multi-cycle E-peroxone process than during the multi-cycle EGH process (see Fig. 4 and Table 1), which can be

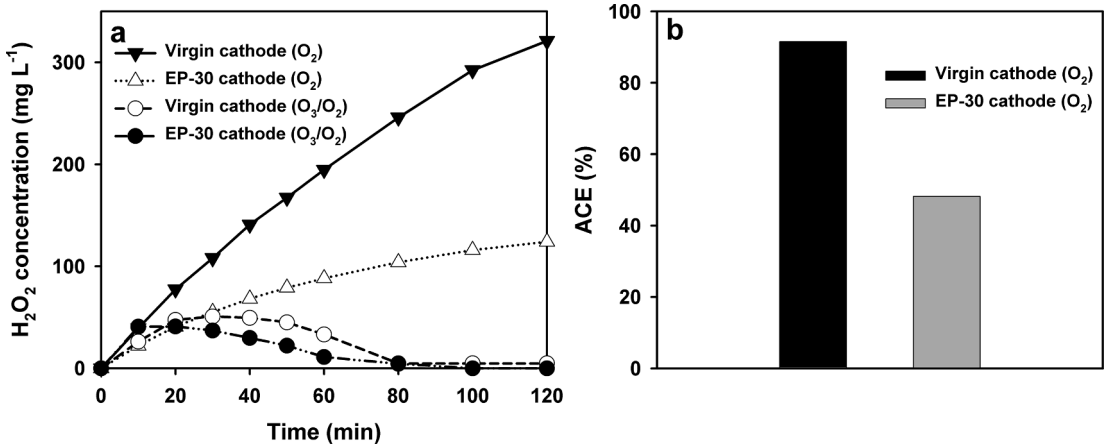

Fig. 7. (a) Evolution of H_2O_2 concentration during electrochemical generation of H_2O_2 (pure O_2 sparging) and E-peroxone treatment of phenol solutions (O_3/O_2 sparging) with the virgin cathode and the cathode used for 30 cycles of E-peroxone process (EP-30), (b) apparent current efficiency (ACE) for H_2O_2 production during electrochemical generation of H_2O_2 (pure O_2 sparging) with the virgin and EP-30 cathode.

attributed to the more severe oxidation of carbon fiber surface in the presence of O_3. Nevertheless, O_3 is a highly selective oxidant. In addition, upon cathodic polarization, net electrons will accumulate on the carbon fiber surface, which can protect the interior fiber structure from being oxidized by O_3 [30–32]. Therefore, it is expected that after the O_3-reactive functional groups on the carbon fiber surface are largely transformed to O_3-resistant groups, further oxidation of the bulk carbon fibers by O_3 will be insignificant under the cathodic polarization conditions. Consistently, carbon fiber characterizations by the various techniques (e.g., elemental analysis, SEM, XPS, and FT-IR) demonstrate that except the exfoliation of epoxy resin coating and transformation of surface N-containing groups, there were no significant changes in the shape, size, and morphology of the bulk carbon fibers after the electrode was used for 30 cycles of the E-peroxone process with the highest ozone exposure (O_3 = 90 mg L^{-1}). Moreover, LSV analysis showed that after the initial significant shift of LSV curve of the EP-1 cathode, the LSV curves did not further change considerably as the carbon brush cathode was repeatedly used in the E-peroxone process (Fig. 3). These observations suggest that after the initial quick changes, the carbon brush cathode seems to reached a relatively stable state under the counteractive effects of O_3/H_2O_2 oxidation and cathodic reduction during the multi-cycle E-peroxone process. Consequently, similar phenol mineralization efficiencies were generally obtained during the 30 cycles of the E-peroxone process. Overall, the results of this study suggest that the polyacrylonitrile-based carbon fiber cathode can be possibly used for a long period and maintain a high stability for pollutant removal during the E-peroxone process. To more realistically assess the economic feasibility of the carbon brush electrode for electrochemical H_2O_2 production, further studies are needed to evaluate the long-term performance and lifetime of the electrode under realistic water treatment conditions.

4. Conclusions

Polyacrylonitrile-based carbon fiber was used as the cathode material for electrochemical generation of H_2O_2 (EGH) with pure O_2 sparging and the E-peroxone treatment of phenol solutions with O_3/O_2 sparging. The exposures of carbon fibers to electro-generated H_2O_2 and/or bubbled O_3 during the EGH and E-peroxone processes caused oxidation of the carbon fiber surface. As a result, N-containing groups on the carbon fiber surface were increasingly exposed and converted from pyridinic-N to pyridonic-N as the carbon brush cathode was continuously used in the processes. These changes resulted in an increase in the ORR activity of the carbon brush cathode, but a decrease in the selectivity of the cathode for two-electron ORR to H_2O_2. Consequently, the cathodic potential for ORR shifted positively, whereas the ACE for H_2O_2 decreased during the multi-cycle EGH and EP processes. Overall, the polyacrylonitrile-based carbon fiber cathode maintained high stability for H_2O_2 production at relatively low energy consumption and high phenol mineralization efficiency during the multi-cycle EGH and E-peroxone processes, respectively. These results suggest that polyacrylonitrile-based carbon fiber is a promising cathode material for long-term E-peroxone operations.

Declaration of Competing Interest

The authors declare that they have no known competing financial interests or personal relationships that could have appeared to influence the work reported in this paper.

Acknowledgements

We acknowledge financial support from the National Natural Science Foundation of China (51878370, 51572296, U1662113), China Postdoctoral Science Foundation (2016M601054, 2017M622320), National Special Program of Water Pollution Control and Management (No. 2017ZX07202), Taishan Scholar Project (ts201712020), Beijing Key Laboratory for Emerging Organic Contaminants Control Open Fund.

Appendix A. Supplementary data

Supplementary data to this article can be found online at https://doi.org/10.1016/j.cej.2020.125291.

References

[1] S. Yuan, Z.X. Li, Y.J. Wang, Effective degradation of methylene blue by a novel electrochemically driven process, Electrochem. Commun. 29 (2013) 48–51.
[2] Y. Wang, G. Yu, S. Deng, J. Huang, B. Wang, The electro-peroxone process for the abatement of emerging contaminants: mechanisms, recent advances, and prospects, Chemosphere 208 (2018) 640–654.
[3] O. Turkay, S. Barisci, B. Ozturk, H. Ozturk, A. Dimoglo, Electro-peroxone treatment of phenol: process comparison, the effect of operational parameters and degradation mechanism, J. Electrochem. Soc. 164 (2017) E180–E186.
[4] Y. Li, Y. Ma, G. Xia, G. Yu, Y. Wang, Evaluation of the feasibility of electrochemical hydrogen peroxide production for practical water treatment, Submitted (2020).
[5] W. Yao, J. Fu, H. Yang, G. Yu, Y. Wang, The beneficial effect of cathodic hydrogen peroxide generation on mitigating chlorinated by-product formation during water treatment by an electro-peroxone process, Water Res. 157 (2019) 209–217.
[6] O. Turkay, Z.G. Ersoy, S. Barisci, Review—The application of an electro-peroxone process in water and wastewater treatment, J. Electrochem. Soc. 164 (2017) E94–E102.
[7] B. Bakheet, S. Yuan, Z. Li, H. Wang, J. Zuo, S. Komarneni, Y. Wang, Electro-peroxone treatment of Orange II dye wastewater, Water Res. 47 (2013) 6234–6243.
[8] W. Yao, S.W. Ur Rehman, H. Wang, H. Yang, G. Yu, Y. Wang, Pilot-scale evaluation of micropollutant abatements by conventional ozonation, UV/O_3, and an electro-peroxone process, Water Res. 138 (2018) 106–117.
[9] W. Yao, Q. Qu, U. von Gunten, C. Chen, G. Yu, Y. Wang, Comparison of methylisoborneol and geosmin abatement in surface water by conventional ozonation and an electro-peroxone process, Water Res. 108 (2017) 373–382.
[10] H. Wang, J. Zhan, W. Yao, B. Wang, S. Deng, J. Huang, G. Yu, Y. Wang, Comparison of pharmaceutical abatement in various water matrices by conventional ozonation, peroxone (O_3/H_2O_2), and an electro-peroxone process, Water Res. 130 (2018) 127–138.
[11] U. von Gunten, Y. Oliveras, Kinetics of the reaction between hydrogen peroxide and hypobromous acid: implication on water treatment and natural systems, Water Res. 31 (1997) 900–906.
[12] Y.K. Li, W.H. Shen, S.J. Fu, H.W. Yang, G. Yu, Y.J. Wang, Inhibition of bromate formation during drinking water treatment by adapting ozonation to electro-peroxone process, Chem. Eng. J. 264 (2015) 322–328.
[13] Y. Guo, E. Zhao, J. Wang, X. Zhang, H. Huang, G. Yu, Y. Wang, Comparison of emerging contaminant abatement by conventional ozonation, catalytic ozonation, O_3/H_2O_2 and electro-peroxone processes, J. Hazard. Mater. (2020) 121829.
[14] Y. Mao, D. Guo, W. Yao, X. Wang, H. Yang, Y.F. Xie, S. Komarneni, G. Yu, Y. Wang, Effects of conventional ozonation and electro-peroxone pretreatment of surface water on disinfection by-product formation during subsequent chlorination, Water Res. 130 (2018) 322–332.
[15] Z. Lu, G. Chen, S. Siahrostami, Z. Chen, K. Liu, J. Xie, L. Liao, T. Wu, D. Lin, Y. Liu, T.F. Jaramillo, J.K. Nørskov, Y. Cui, High-efficiency oxygen reduction to hydrogen peroxide catalysed by oxidized carbon materials, Nat. Catal. 1 (2018) 156–162.
[16] E. Brillas, I. Sires, M.A. Oturan, Electro-Fenton process and related electrochemical technologies based on Fenton's reaction chemistry, Chem. Rev. 109 (2009) 6570–6631.
[17] S. Yang, A. Verdaguer-Casadevall, L. Arnarson, L. Silvioli, V. Čolić, R. Frydendal, J. Rossmeisl, I. Chorkendorff, I.E.L. Stephens, Toward the decentralized electrochemical production of H_2O_2: a focus on the catalysis, ACS Catal. 8 (2018) 4064–4081.
[18] I. Sires, E. Guivarch, N. Oturan, M.A. Oturan, Efficient removal of triphenylmethane dyes from aqueous medium by in situ electrogenerated Fenton's reagent at carbon-felt cathode, Chemosphere 72 (2008) 592–600.
[19] N. Oturan, C.T. Aravindakumar, H. Olvera-Vargas, M.M. Sunil Paul, M.A. Oturan, Electro-Fenton oxidation of para-aminosalicylic acid: degradation kinetics and mineralization pathway using Pt/carbon-felt and BDD/carbon-felt cells, Environ. Sci. Pollut. Res. 25(2018) 20363-20373.
[20] I. Salmerón, K.V. Plakas, I. Sirés, I. Oller, M.I. Maldonado, A.J. Karabelas, S. Malato, Optimization of electrocatalytic H_2O_2 production at pilot plant scale for solar-assisted water treatment, Appl. Catal. B: Environ. 242 (2019) 327–336.
[21] D.H. Wu, G.H. Lu, R. Zhang, Q.H. Lin, J.J. Yao, X.H. Shen, W. Wang, Effective degradation of diatrizoate by electro-peroxone process using ferrite/carbon nanotubes based gas diffusion cathode, Electrochim. Acta 236 (2017) 389–398.
[22] M. Hou, Y. Chu, X. Li, H. Wang, W. Yao, G. Yu, S. Murayama, Y. Wang, Electro-peroxone degradation of diethyl phthalate: cathode selection, operational parameters, and degradation mechanisms, J. Hazard. Mater. 319 (2016) 61–68.
[23] G. Xia, Y. Wang, B. Wang, J. Huang, S. Deng, G. Yu, The competition between cathodic oxygen and ozone reduction and its role in dictating the reaction mechanisms of an electro-peroxone process, Water Res. 118 (2017) 26–38.

[24] N. Bensalah, A. Bedoui, Enhancing the performance of electro-peroxone by incorporation of UV irradiation and BDD anodes, Environ. Technol. 38 (2017) 2979–2987.
[25] I. Bavasso, D. Montanaro, L. Di Palma, E. Petrucci, Electrochemically assisted decomposition of ozone for degradation and mineralization of Diuron, Electrochim. Acta 331 (2020) 135423.
[26] T.X.H. Le, C. Charmette, M. Bechelany, M. Cretin, Facile preparation of porous carbon cathode to eliminate paracetamol in aqueous medium using electro-Fenton system, Electrochim. Acta 188 (2016) 378–384.
[27] T.X.H. Le, R. Esmilaire, M. Drobek, M. Bechelany, C. Vallicari, S. Cerneaux, A. Julbe, M. Cretin, Nitrogen-doped graphitized carbon electrodes for biorefractory pollutant removal, J. Phys. Chem. C 121 (2017) 15188–15197.
[28] A. Khataee, S. Sajjadi, S.R. Pouran, A. Hasanzadeh, S.W. Joo, A comparative study on electrogeneration of hydrogen peroxide through oxygen reduction over various plasma-treated graphite electrodes, Electrochim. Acta 244 (2017) 38–46.
[29] M. Sánchez-Polo, U. von Gunten, J. Rivera-Utrilla, Efficiency of activated carbon to transform ozone into OH radicals: influence of operational parameters, Water Res. 39 (2005) 3189–3198.
[30] J.H. Zhan, Y.J. Wang, H.J. Wang, W.H. Shen, X.J. Pan, J.L. Wang, G. Yu, Electro-peroxone regeneration of phenol-saturated activated carbon fiber: the effects of irreversible adsorption and operational parameters, Carbon 109 (2016) 321–330.
[31] J.H. Zhan, H.J. Wang, X.J. Pan, J.L. Wang, G. Yu, S.B. Deng, J. Huang, B. Wang, Y.J. Wang, Simultaneous regeneration of p-nitrophenol-saturated activated carbon fiber and mineralization of desorbed pollutants by electro-peroxone process, Carbon 101 (2016) 399–408.
[32] X.K. Zhang, Y. Zhou, C. Zhao, Z.H. Sun, Z.G. Zhang, Z.A. Mirza, G. Saylor, J. Zhai, H.L. Zheng, Electric field induced activated carbon fiber (ACF) cathode transition from an initiator/a promoter into an electrocatalyst in ozonation process, Chem. Eng. J. 304 (2016) 129–133.
[33] J. Lu, W. Li, H. Kang, L. Feng, J. Xu, R. Liu, Microstructure and properties of polyacrylonitrile based carbon fibers, Polym. Test. 81 (2020) 106267.
[34] J.H. Park, G.C. Rutledge, 50th anniversary perspective: advanced polymer fibers: high performance and ultrafine, Macromolecules 50 (2017) 5627–5642.
[35] H. Xu, G. Xia, H. Liu, S. Xia, Y. Lu, Electrochemical activation of commercial polyacrylonitrile-based carbon fiber for the oxygen reduction reaction, Phys. Chem. Chem. Phys. 17 (2015) 7707–7713.
[36] H. Xu, Y. Lu, C. Li, J. Hu, A novel IrO_2 electrode with iridium–titanium oxide interlayers from a mixture of TiN nanoparticle and H_2IrCl_6 solution, J. Appl. Electrochem. 40 (2009) 719–727.
[37] G. Xia, Y. Lu, H. Xu, Electrogeneration of hydrogen peroxide for electro-Fenton via oxygen reduction using polyacrylonitrile-based carbon fiber brush cathode, Electrochim. Acta 158 (2015) 390–396.
[38] R.M. Sellers, Spectrophotometric determination of hydrogen peroxide using potassium titanium(IV) oxalate, Analyst 105 (1980) 950–954.
[39] H. Bader, J. Hoigné, Determination of ozone in water by the indigo method, Water Res. 15 (1981) 449–456.
[40] R.A. Mir, O.P. Pandey, Influence of graphitic/amorphous coated carbon on HER activity of low temperature synthesized β-Mo_2C@C nanocomposites, Chem. Eng. J. 348 (2018) 1037–1048.
[41] D. Voiry, M. Chhowalla, Y. Gogotsi, N.A. Kotov, Y. Li, R.M. Penner, R.E. Schaak, P.S. Weiss, Best practices for reporting electrocatalytic performance of nanomaterials, ACS Nano 12 (2018) 9635–9638.
[42] Y. Meng, W. Song, H. Huang, Z. Ren, S.-Y. Chen, S.L. Suib, Structure–property relationship of bifunctional MnO_2 nanostructures: highly efficient, ultra-stable electrochemical water oxidation and oxygen reduction reaction catalysts identified in alkaline media, J. Am. Chem. Soc. 136 (2014) 11452–11464.
[43] S. Siahrostami, A. Verdaguer-Casadevall, M. Karamad, D. Deiana, P. Malacrida, B. Wickman, M. Escudero-Escribano, E.A. Paoli, R. Frydendal, T.W. Hansen, I. Chorkendorff, I.E.L. Stephens, J. Rossmeisl, Enabling direct H_2O_2 production through rational electrocatalyst design, Nat. Mater. 12 (2013) 1137–1143.
[44] B. Logan, S. Cheng, V. Watson, G. Estadt, Graphite fiber brush anodes for increased power production in air-cathode microbial fuel cells, Environ. Sci. Technol. 41 (2007) 3341–3346.
[45] M. Qiao, M.M. Titirici, Engineering the interface of carbon electrocatalysts at the triple point for enhanced oxygen reduction reaction, Chem. Eur. J. 24 (2018) 18374–18384.
[46] USEIA, Annual Electric Sales, Revenue, and Average Price, (2016) form: http://www.eia.gov/electricity/sales_revenue_price/.
[47] J.M. Barazesh, T. Hennebel, J.T. Jasper, D.L. Sedlak, Modular advanced oxidation process enabled by cathodic hydrogen peroxide production, Environ. Sci. Technol. 49 (2015) 7391–7399.
[48] E. Pamula, P.G. Rouxhet, Bulk and surface chemical functionalities of type III PAN-based carbon fibres, Carbon 41 (2003) 1905–1915.
[49] L. Meng, D. Fan, Y. Huang, Z. Jiang, C. Zhang, Comparison studies of surface cleaning methods for PAN-based carbon fibers with acetone, supercritical acetone and subcritical alkali aqueous solutions, Appl. Surf. Sci. 261 (2012) 415–421.
[50] T. Palaniselvam, M.O. Valappil, R. Illathvalappil, S. Kurungot, Nanoporous graphene by quantum dots removal from graphene and its conversion to a potential oxygen reduction electrocatalyst via nitrogen doping, Energy Environ. Sci. 7 (2014) 1059–1067.
[51] R. Silva, D. Voiry, M. Chhowalla, T. Asefa, Efficient metal-free electrocatalysts for oxygen reduction: polyaniline-derived N- and O-doped mesoporous carbons, J. Am. Chem. Soc. 135 (2013) 7823–7826.
[52] A. Achour, S. Vizireanu, G. Dinescu, L. Le Brizoual, M.A. Djouadi, M. Boujtita, Electrochemical anodic oxidation of nitrogen doped carbon nanowall films: X-ray photoelectron and Micro-Raman spectroscopy study, Appl. Surf. Sci. 273 (2013) 49–57.
[53] D. Guo, R. Shibuya, C. Akiba, S. Saji, T. Kondo, J. Nakamura, Active sites of nitrogen-doped carbon materials for oxygen reduction reaction clarified using model catalysts, Science 351 (2016) 361–365.
[54] D.-W. Wang, F. Li, L.-C. Yin, X. Lu, Z.-G. Chen, I.R. Gentle, G.Q. Lu, H.-M. Cheng, Nitrogen-doped carbon monolith for alkaline supercapacitors and understanding nitrogen-induced redox transitions, Chem. Eur. J. 18 (2012) 5345–5351.
[55] P. Su, M. Zhou, X. Lu, W. Yang, G. Ren, J. Cai, Electrochemical catalytic mechanism of N-doped graphene for enhanced H_2O_2 yield and in-situ degradation of organic pollutant, Appl. Catal. B: Environ. 245 (2019) 583–595.
[56] Y.Y. Sun, I. Sinev, W. Ju, A. Bergmann, S. Dresp, S. Kuhl, C. Spori, H. Schmies, H. Wang, D. Bernsmeier, B. Paul, R. Schmack, R. Kraehnert, B. Roldan Cuenya, P. Strasser, Efficient electrochemical hydrogen peroxide production from molecular oxygen on nitrogen-doped mesoporous carbon catalysts, ACS Catal. 8 (2018) 2844–2856.
[57] H. Wang, S. Yuan, J. Zhan, Y. Wang, G. Yu, S. Deng, J. Huang, B. Wang, Mechanisms of enhanced total organic carbon elimination from oxalic acid solutions by electro-peroxone process, Water Res. 80 (2015) 20–29.
[58] M. Panizza, G. Cerisola, Direct and mediated anodic oxidation of organic pollutants, Chem. Rev. 109 (2009) 6541–6569.
[59] C. von Sonntag, U. von Gunten, Chemistry of Ozone in Water and Wastewater Treatment. From Basic Principles to Applications, IWA Publishing, 2012.
[60] J. Restivo, E. Garcia-Bordeje, J.J.M. Orfao, M.F.R. Pereira, Carbon nanofibers doped with nitrogen for the continuous catalytic ozonation of organic pollutants, Chem. Eng. J. 293 (2016) 102–111.

Supporting Information

Evaluation of the stability of polyacrylonitrile-based carbon fiber electrode for hydrogen peroxide production and phenol mineralization during electro-peroxone process

Guangsen Xia[1 2], Huijiao Wang[2], Juhong Zhan[2], Xiaomeng Yin[1], Xiaocui Wu[1], Gang Yu[2], Yujue Wang[2]*, Mingbo Wu[1]*

[1] State Key Laboratory of Heavy Oil Processing, College of New Energy, College of Chemical Engineering, China University of Petroleum (East China), Qingdao 266580, China

[2] School of Environment, State Key Joint Laboratory of Environmental Simulation and Pollution Control, Beijing Key Laboratory for Emerging Organic Contaminants Control, Tsinghua University, Beijing 100084, China

* Corresponding author: Yujue Wang; E-mail: wangyujue@tsinghua.edu.cn

Mingbo Wu; E-mail: wumb@upc.edu.cn

S1. Electrochemical H_2O_2 production

Energy consumption (EC; kWh kg^{-1}) for H_2O_2 electro-generation from ORR can be calculated according to Eqs. (S1 and S2), where E_{cel} is the cell voltage (V), I is the applied current (A), t is the electrolysis time (h), m is the mass of the electrogenerated H_2O_2 (kg), V is the solution volume (L), $C(H_2O_2)$ is the H_2O_2 concentration after electrolysis of 20 min.

$$\mathrm{EC} = \frac{IE_{cel}t}{1000m} \qquad \text{(S1)}$$

$$\mathrm{m}=10^{-6}\, VC(H_2O_2) \qquad \text{(S2)}$$

Table S1 Energy consumption for H_2O_2 production during electrolysis with the virgin cathode and the cathode used for 30 cycles of electrochemical generation of H_2O_2.

Cathode	I (A)	E_{cel} (V)	T (h)	$C(H_2O_2)$ (mg/L)	V (L)	EC (kWh kg^{-1})
Virgin cathode	0.4	3.5	1/3	81.86	1	5.7
EGH-30 cathode	0.4	3.2	1/3	66.80	1	6.4

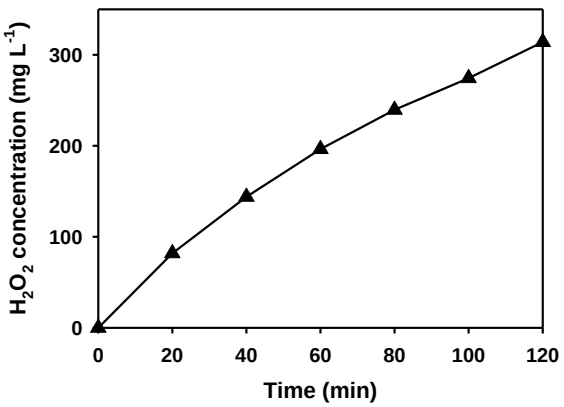

Fig. S1. Evolution of H_2O_2 concentration with increasing electrolysis time.

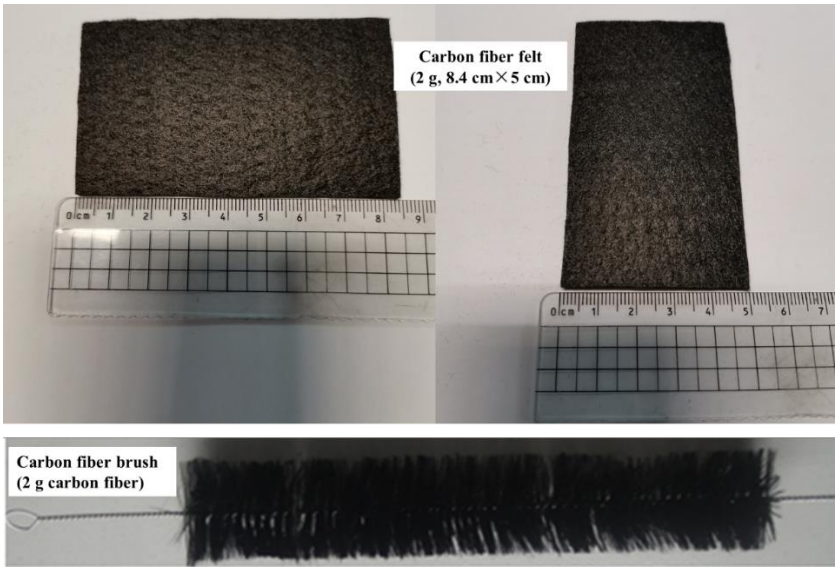

Fig. S2. Photos of polyacrylonitrile-based carbon felt and carbon brush electrode.

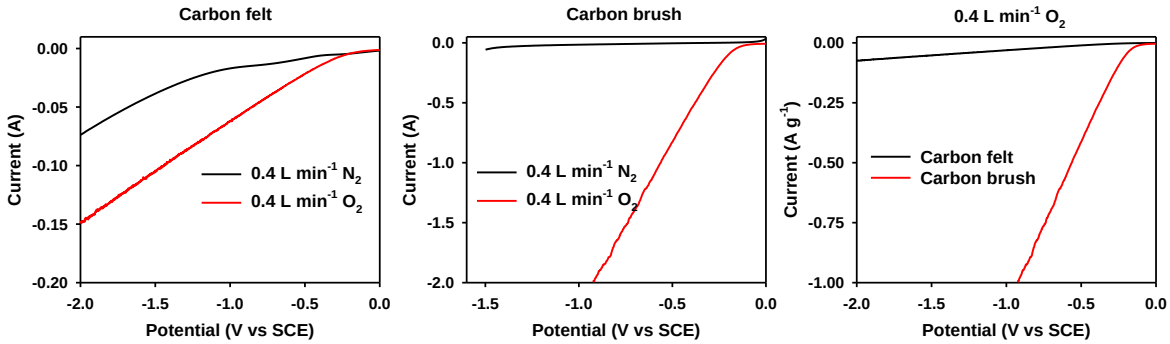

Fig. S3. LSV curves of carbon felt and carbon brush cathode in Na_2SO_4 electrolyte sparged with pure N_2 and O_2 gas (Na_2SO_4 concentration = 0.1 mol L^{-1}, scanning rate = 10 mV s^{-1}, gas flow rate = 0.4 L min^{-1}).

Table S2. Comparison of electrochemical H_2O_2 production with various carbon-based cathodes.

Cathode	Experimental conditions	H_2O_2 production rate (mg h^{-1})	ACE (%)	Reference
CB-PTFE	V = 0.4 L, O_2 flow rate = 0.4 L min^{-1}, current = 400 mA	202	80	[1]
RVC	V = 0.4 L, O_2 flow rate = 0.4 L min^{-1}, current = 400 mA	136	55	[1]
Carbon felt	V = 0.4 L, O_2 flow rate = 0.4 L min^{-1}, current = 400 mA	101	40	[1]
Carbon brush	V = 0.4 L, O_2 flow rate = 0.4 L min^{-1}, current = 400 mA	228	90	This work

S2. Phenol removal by adsorption, anodic oxidation, and the E-peroxone process

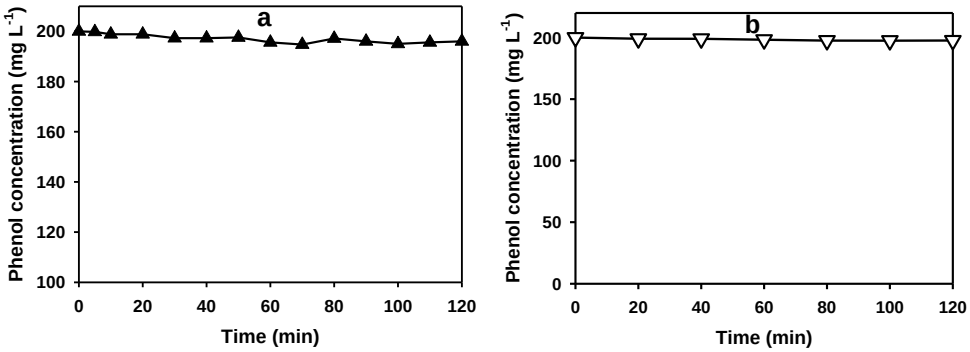

Fig. S4. Phenol removal by (a) adsorption with the carbon brush cathode and (b) anodic oxidation with the Ti/IrO_2 anode. (Na_2SO_4 concentration = 0.1 mol L^{-1}, the current for anodic oxidation is 400 mA and a stainless steel sheet is used as cathode with merely hydrogen evolution reaction in the solution removing oxygen by sparging pure N_2 gas at a flow rate of 0.4 L min^{-1})

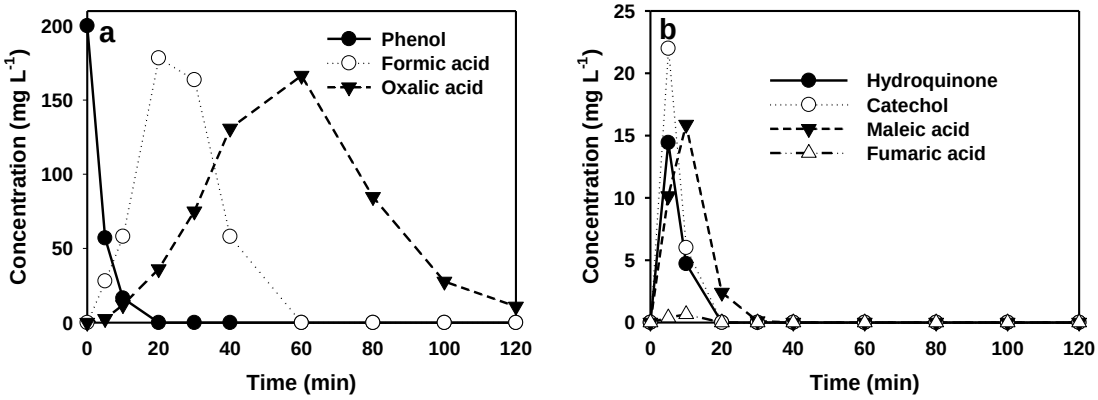

Fig. S5 Evolution of phenol and its transformation products during E-peroxone treatment of phenol solution (Na_2SO_4 concentration = 0.1 mol L^{-1}, current = 400 mA, gas phase O_3 concentration = 90 mg L^{-1}, gas flow rate = 0.4 L min^{-1})

S3. Carbon fiber characterizations

The surface morphology of the virgin cathode and the cathodes used for 30 cycles of EGH and EP test were examined using scanning electron microscopy (SEM). As shown in Fig. S6, there were insignificant changes in the shape and size of the fibers after the multi-cycle EGH and EP processes. These observations indicate that the oxidation of bulk fiber by H_2O_2 and/or O_3 is negligible during the EGH and EP process, consistent with the results of bulk elemental composition analysis (Table 1). Nevertheless, a more smooth surface was observed for the fibers of the EGH-30 and EP-30 cathodes than the virgin cathode (see Figs. S6c, f, and i), which can be attributed to the exfoliation of sizing agent coating (epoxy resin) during the EGH and EP process. The removal of insulating epoxy resin coating from the carbon fiber surface facilitates electron transfers between the cathode and electrolyte [2, 3], and thus enhanced the ORR activity of the EGH-30 and EP-30 electrode (see Fig. 3).

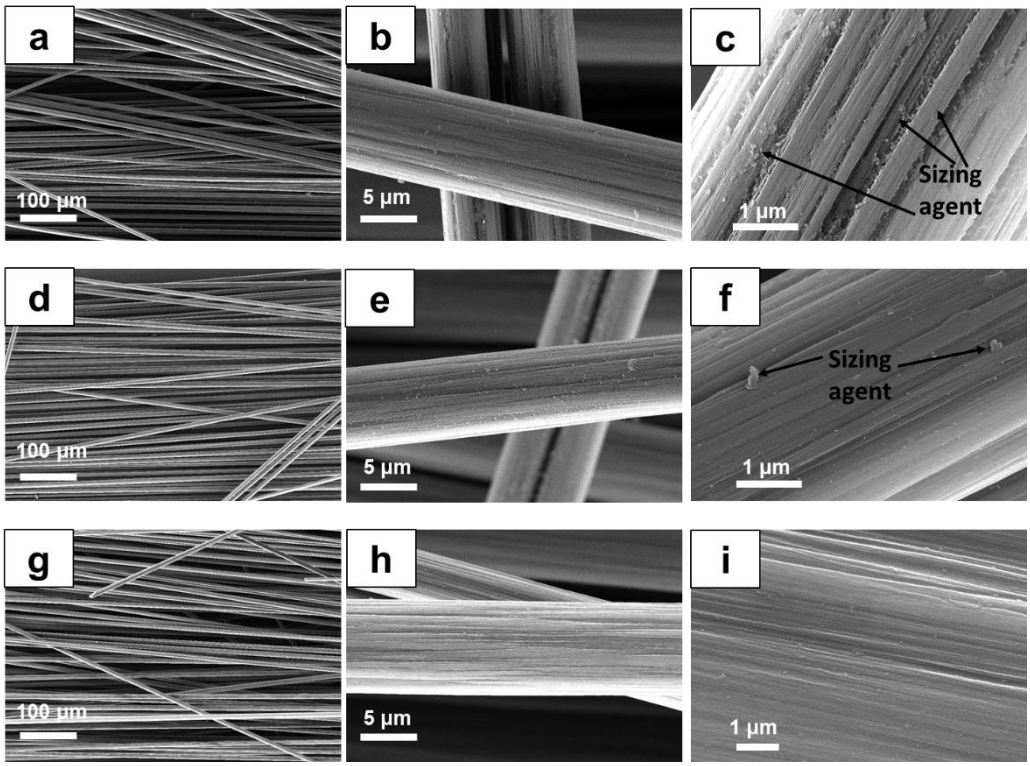

Fig. S6. SEM images of carbon fibers on the (a, b, c) virgin, (d, e, f) EGH-30, and (g, h, i) EP-30 cathodes.

The FT-IR spectra of carbon fibers of the virgin, EGH-30, and EP-30 cathodes are compared in Fig. S7. The characteristic peaks at 3440, 2915/2850, 1630, 1090, 802 cm^{-1} can be ascribed to O-H stretching vibration, C-H stretching vibration of $-CH_2$, C=C stretching vibration, C-O-C stretching vibration, and C-H bending vibration of C=C-H, respectively [4-6]. Compared with the virgin fibers, the most notable change in the FT-IR spectra of the EGH-30 and EP-30 fibers is the significant decrease in the peak at 1090 cm^{-1}. This change can be possibly attributed to the exfoliation of epoxy resin coating from the carbon fiber during the multi-cycle EGH and EP test, which will reduce the intensity of C-O-C stretching vibration of the used carbon fibers [7]. For the other peaks, the intensities are generally similar for the fibers on the virgin and used cathodes, which suggests that the oxidation of bulk fibers is insignificant during the multi-cycle EGH and EP processes.

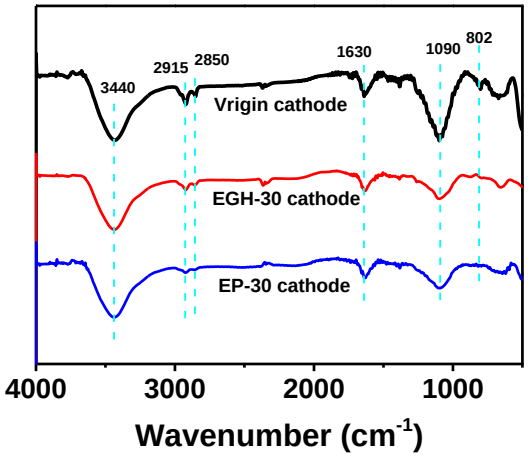

Fig. S7. FT-IR spectra of carbon fiber on virgin, EGH-30 and EP-30 cathode

XRD analysis shows that the diffraction peak of carbon fiber at $2\theta = 25.4°$ (a peak ascribed to disordered graphitic (002) plane) [8] decreased moderately after the carbon fiber cathode was used for 30 cycles of the EGH and EP test (Fig. S8). Moreover, the crystallite size of carbon fiber also decreased slightly from 12.7 Å for the virgin cathode to 12.3 and 12.2 Å for the EGH-30 and EP-30 cathode, respectively (calculated according to the XRD pattern and

Scherrer's formula [9]). These changes indicate that the original turbostratic graphite structure of carbon fiber was weakly damaged by the oxidation of H_2O_2 and/or O_3 during the multi-cycle of EGH and EP process [8, 9].

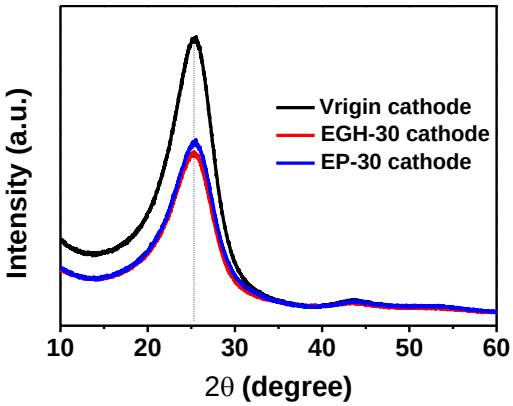

Fig. S8. XRD pattern of carbon fiber on the virgin, EGH-30, and EP-30 cathodes.

Fig. S9 shows that the virgin carbon fiber exhibits two characteristic bands at 1360 cm^{-1} (D band) and 1580 cm^{-1} (G band) in the Raman spectra. The D band is attributed to A_{1g} symmetry vibration related to the defects or disorders of graphitic lattices, whereas the G band is corresponding to an ideal graphitic lattice vibration mode with E_{2g} symmetry [7, 10]. Therefore, the intensity ratio of the D and G bands (I_D/I_G) is often used as an indicator for the carbon graphitization or disorder degree [7, 8]. Due to the exposure to H_2O_2 and/or O_3, the I_D/I_G ratio increased from 0.93 for the fibers on the virgin cathode to 1.02 for those on the EGH-30 and EP-30 cathodes. These data suggest that the graphitization degree of the carbon fibers decreased as the cathode was repeatedly used in the EGH and EP processes, consistent with the XRD results.

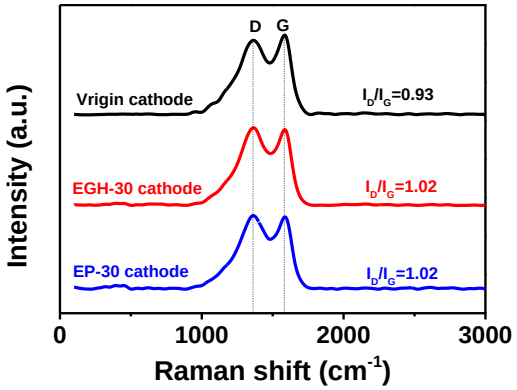

Fig. S9. Raman spectra of carbon fibers on the virgin, EGH-30, and EP-30 cathodes.

The electrochemical double-layer capacitance (EDLC, C_{dl}) of the virgin, EGH-30, EP-30 cathodes were measured from the cyclic voltammetry (CV) in the potential range of 0.15–0.3 V vs. SCE, a typical non-Faradaic region where no charge-transfer reactions occur but absorption and desorption processes can take place (Figs. S10a-c). Based on the linear relationship between the scanning rate and non-Faradaic current density, the C_{dl} of the electrode can then be estimated from the slope of linear regression ($C_{dl} = \frac{j}{v}$) (Fig. S10d). As shown, the C_{dl} value increased remarkably from 27 mF for the virgin cathode to 183 and 237 mF for the EGH-30 and EP-30 cathode, respectively. As the C_{dl} of electrode is directly proportional to the electrochemically active surface area (ECSA) of the solid-liquid interface during electrolysis [11, 12], the significant increase in the C_{dl} value indicate the EGH-30 and EP-30 cathode have much larger ECSA than the virgin cathode. These changes can be possibly attributed to the removal of epoxy resin coating and oxidation of carbon fiber surface by H_2O_2/O_3, which increase the hydrophilicity of carbon fibers and thus facilitates the wetting of electrode during electrolysis [13]. The increase of ECSA facilitates DO and electron transfer between the electrolyte and the electrode [9], and thus enhanced the ORR activity of the EGH-30 and EP-30 cathodes compared to the virgin cathode (Fig. 3).

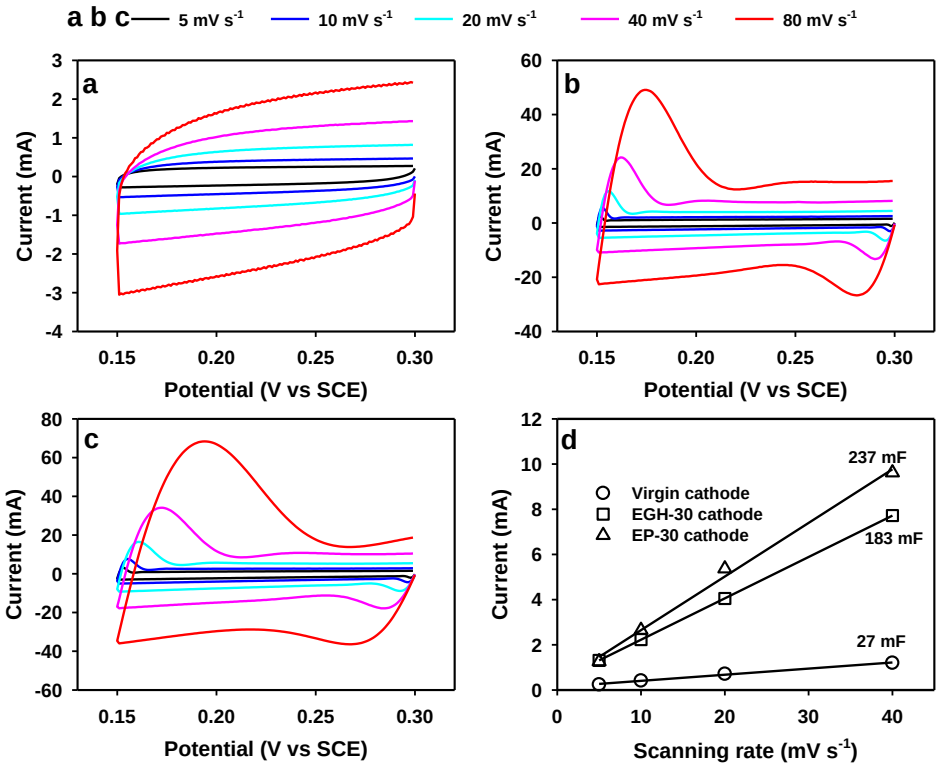

Fig. S10. Cyclic voltammetry (CV) at different scanning rates (a) virgin cathode, (b) EGH-30 cathode, (c) EP-30 cathode and their (d) electrical double-layer capacitance (EDLC)

The electrochemical impedance spectroscopy of the virgin, EGH-30, and EP-30 cathodes was measured under ORR conditions (Fig. S11). The resistance shown in the high frequency region is related to the solution resistance (R_s, ohmic resistance), which was found to be similar for the three cathodes (Table 1). In contrast, the charge transfer resistances (R_{ct}) obtained from the fitted equivalent circuit decreased dramatically from 28.85 Ω for the virgin cathode to 0.31 and 0.30 Ω for the EGH-30 and EP-30 cathodes (Table 1). These decreases can be probably attributed to the removal of insulating epoxy resin coating and the exposure of N-containing groups, which facilitate electron transfer between the electrode and electrolyte. Due to the decreased R_{ct}, the activity of ORR increased considerably for the EGH-30 and EP-30 cathodes compared to the virgin cathode, as evidenced by the considerable decrease of cathodic potentials of ORR (Fig. 3c).

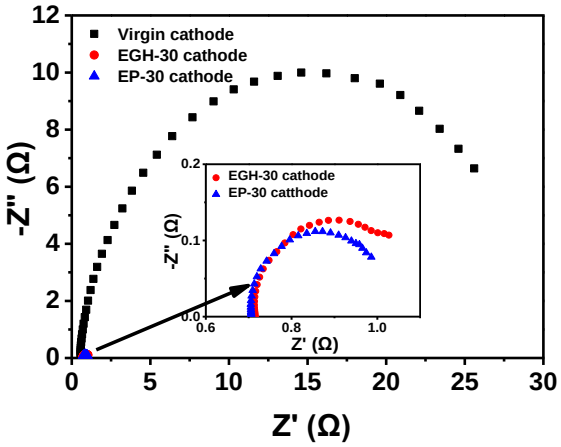

Fig. S11. Nyquist plots obtained from EIS measurements in O_2-saturated 0.1 mol L^{-1} Na_2SO_4 solution on the virgin, EGH-30, and EP-30 cathode at a potential of 0.3 V vs SCE.

References

[1] M. Hou, Y. Chu, X. Li, H. Wang, W. Yao, G. Yu, S. Murayama, Y. Wang, Electro-peroxone degradation of diethyl phthalate: Cathode selection, operational parameters, and degradation mechanisms, J. Hazard. Mater. 319 (2016) 61-68.

[2] E. Pamula, P.G. Rouxhet, Bulk and surface chemical functionalities of type III PAN-based carbon fibres, Carbon 41 (2003) 1905-1915.

[3] L. Meng, D. Fan, Y. Huang, Z. Jiang, C. Zhang, Comparison studies of surface cleaning methods for PAN-based carbon fibers with acetone, supercritical acetone and subcritical alkali aqueous solutions, Appl. Surf. Sci. 261 (2012) 415-421.

[4] J. Jiang, X. Yao, C. Xu, Y. Su, L. Zhou, C. Deng, Influence of electrochemical oxidation of carbon fiber on the mechanical properties of carbon fiber/graphene oxide/epoxy composites, Composites Part A: Applied Science and Manufacturing 95 (2017) 248-256.

[5] X. Yao, X. Gao, J. Jiang, C. Xu, C. Deng, J. Wang, Comparison of carbon nanotubes and graphene oxide coated carbon fiber for improving the interfacial properties of carbon

fiber/epoxy composites, Composites Part B: Engineering 132 (2018) 170-177.

[6] C. Zhang, R. Li, J. Liu, S. Guo, L. Xu, S. Xiao, Z. Shen, Hydrogen peroxide modified polyacrylonitrile-based fibers and oxidative stabilization under microwave and conventional heating – The 1st comparative study, Ceram. Int. 45 (2019) 13385-13392.

[7] P. Kainourgios, I.A. Kartsonakis, D.A. Dragatogiannis, E.P. Koumoulos, P. Goulis, C.A. Charitidis, Electrochemical surface functionalization of carbon fibers for chemical affinity improvement with epoxy resins, Appl. Surf. Sci. 416 (2017) 593-604.

[8] H. Xu, G. Xia, H. Liu, S. Xia, Y. Lu, Electrochemical activation of commercial polyacrylonitrile-based carbon fiber for the oxygen reduction reaction, Phys. Chem. Chem. Phys. 17 (2015) 7707-7713.

[9] T.X.H. Le, C. Charmette, M. Bechelany, M. Cretin, Facile Preparation of Porous Carbon Cathode to Eliminate Paracetamol in Aqueous Medium Using Electro-Fenton System, Electrochim. Acta 188 (2016) 378-384.

[10] L. Liu, F. Wu, H. Yao, J. Shi, L. Chen, Z. Xu, H. Deng, Investigation of surface properties of pristine and γ-irradiated PAN-based carbon fibers: Effects of fiber instinct structure and radiation medium, Appl. Surf. Sci. 337 (2015) 241-248.

[11] D. Cui, L.-M. Yang, W.-Z. Liu, M.-H. Cui, W.-W. Cai, A.-J. Wang, Facile fabrication of carbon brush with reduced graphene oxide (rGO) for decreasing resistance and accelerating pollutants removal in bio-electrochemical systems, J. Hazard. Mater. 354 (2018) 244-249.

[12] D. Voiry, M. Chhowalla, Y. Gogotsi, N.A. Kotov, Y. Li, R.M. Penner, R.E. Schaak, P.S. Weiss, Best Practices for Reporting Electrocatalytic Performance of Nanomaterials, ACS nano 12 (2018) 9635-9638.

[13] M. Qiao, M.M. Titirici, Engineering the interface of carbon electrocatalysts at the triple point for enhanced Oxygen Reduction Reaction, Chemistry–A European Journal 24 (2018) 18374-18384.